RSCPublishing Faraday Discussions

Application of Twin Screw Extrusion to the Manufacture of Cocrystals: Scale up of AMG 517-Sorbic acid cocrystal production

Journal:	*Faraday Discussions*
Manuscript ID:	FD-ART-12-2013-000153.R1
Article Type:	Paper
Date Submitted by the Author:	07-Feb-2014
Complete List of Authors:	Daurio, Dominick; Amgen Inc., Small Molecule Process & Product Development Nagapudi, Karthik; Amgen Inc., Small Molecule Process & Product Development Li, Lan; Amgen Inc., Small Molecule Process & Product Development Quan, Peter; Amgen Inc., Small Molecule Process & Product Development Alvarez-Nunez, Fernando; Amgen Inc., Small Molecule Process & Product Development

SCHOLARONE™
Manuscripts

Application of Twin Screw Extrusion to the Manufacture of Cocrystals: Scale up of AMG 517-Sorbic acid cocrystal production

Dominick Daurio, Karthik Nagapudi*, Lan Li, Peter Quan and Fernando-Alvarez Nunez*

ABSTRACT

The application of twin screw extrusion (TSE) in the scale up of cocrystal production was investigated by using AMG 517-sorbic acid as a model system. Extrusion parameters that influenced conversion to the cocrystal such temperature, feed rate and screw speed were investigated. Extent of conversion to the cocrystal was found to have a strong dependence on temperature and a moderate dependence on feed rate and screw speed. Cocrystals made by the TSE process were found to have superior mechanical properties than solution grown cocrystals. Additionally, moving to a TSE process eliminated the need for solvent.

INTRODUCTION

It has long been recognized that understanding and manufacturing the appropriate solid form of active pharmaceutical ingredients (API) is an important part of drug development. To this end, substantial effort is expended in the pharmaceutical industry to understand all possible solid forms of a new chemical entity that is being considered for clinical development. In this arena of solid forms, polymorphs and salts are well known entities while cocrystals have been relatively new entrants. Cocrystals are defined as crystalline materials that are comprised of two or more components that are solids at room temperature (in order to distinguish them from hydrates and solvates) held together by non-covalent forces.[1-3] The distinction between a salt and a cocrystal lies in the fact that there is no proton transfer occurring between the constituents of a cocrystal. There has been an increased interest in cocrystals in the last decade and a number of publications have highlighted the beneficial properties of cocrystals.[4-15] While a lot has been published about how to screen for cocrystals there have been relatively few publications about how to scale up the production of cocrystals. This may be attributed to the fact that cocrystals are only now making their way through clinical pipelines and there is no known example of a marketed cocrystal.

Cocrystals can be prepared by either solvent based methods or solid state methods. Typical solvent-based techniques involve solution or slurry crystallizations. These techniques are similar to crystallization methods used for free form or salts of drug substances and are therefore familiar to chemists and engineers. Solution crystallization, in particular, offers good control of chemical purity and material properties. However, the use of solution crystallization for cocrystal scale up does present challenges as knowledge of the ternary phase diagram between the cocrystal constituents and the solvent is necessary and the measurement of such phase diagrams involves a large number of experiments which may be cumbersome to perform.[16-18] In recent years significant progress has been made towards designing simple procedures for using solution crystallization to scale-up the production of cocrystals.[19, 20] Nevertheless, the

use of solution crystallization for cocrystal scale up is still quite complex. In addition, as with any solution crystallization, drying of solvent from the final product to acceptable levels is required.

Cocrystals have also been traditionally prepared in small scale using solid state techniques such as grinding and sonication. There are many reports of making cocrystals by neat grinding of the constituents in mills. Recently, liquid-assisted grinding has been developed as a more effective method to make cocrystals.[14, 21] Grinding methods avoid challenges associated with kinetic crystallizations and solubility differences between solid starting materials. In addition they can produce phases that cannot be formed by solution crystallization and are environmentally friendly as they avoid the use of solvents. While grinding techniques are attractive methods on small scale they cannot be used to scale up large quantities of cocrystals. In recent publications we have introduced twin screw extrusion (TSE) are a viable solid state technique that overcomes the limitations of grinding techniques and can be used for the production of cocrystals.[22, 23] Using this process we demonstrated the formation production of cocrystals of Caffeine-Oxalic acid, AMG 517-Sorbic acid, Cinnamic acid-Nicotinamide, Theophylline-Citric acid and Carbamezapine-Saccharin. Dhumal et. al. has also reported the use of extrusion to make Ibuprofen-Nicontinamide cocrystals. In this publication, they describe a detailed study of the effect of temperature and processing conditions on cocrystal formation.[24, 25] They confirmed that extrusion was an excellent method of producing cocrystals while at the same time being easily amenable to a quality-by-design (QbD) approach. In this paper, the scale up of AMG 517-sorbic acid cocrystals using TSE is described. The solid state data obtained on cocrystals from the TSE approach (labeled TSEC) is compared with that of cocrystals obtained from standard solution crystallization (labeled SCC) approach. Optimization of the twin screw extrusion process for the scale up of the cocrystal is also described.

EXPERIMENTAL SECTION

AMG 517 freebase and solution crystallized-AMG 517-sorbic acid cocrystal were provided by the Chemical Process R&D group at Amgen Inc.

All other chemicals used in the study were purchased from Sigma-Aldrich company (St.Louis, MO) and were used as-received for milling and extrusion experiments. All solvents used were of analytical grade.

Ball Milling

A Retsch Ball Mill model #MM301 was used to grind cocrystal components in order to obtain reference cocrystal material. In general, about 500 mg of the sample to be milled was placed in a 25-mL chamber with metal grinding balls at room temperature. The vibration frequency of the mill was set at 30 Hz for all experiments. The samples were milled for varying lengths of time between 0 and 60 minutes. Two jars of the same mixture were milled at the same time. About 50 mg of mixture was taken out from each of the 2 jars at 5, 15, 30, 45 and 60 min. Samples after milling were assessed using ^{19}F SSNMR to determine the extent of cocrystallization.

Twin Screw Extrusion (TSE)

A Prism PharmaLab 16mm twin screw extruder (25:1 L/D) was used for all experiments. The extruder has four controllable temperature zones (including the die zone). For these experiments the die zone was not used. Temperature of the extruder barrel was changed from 8 to 135 °C to monitor the effect on cocrystal conversion. Appropriate stoichiometric blends of the starting components were prepared and mixed using a turbula blender for 10 minutes prior to being charged into the extruder. The charge to extruder was done through a Brabender single screw volumetric feeder that fed directly into the extruder hopper. Screw feeding rates from 5 to 15% were explored in this study. The screw configuration was designed for high mixing capacity and long residence time to enhance conversion to cocrystal (c.f. Figure 1). The screw design was setup with alternating 16-mm segments of Zone A and Zone B throughout the barrel. Zone A is a purely conveying zone with minimal mixing capacity. Zone A is a single element, 16 mm in length with a pitch of 7.5 mm. Zone B is a high mixing zone with neutral conveying capacity. Zone B is composed of four distributive elements that are 4 mm in length each for a total of 16 mm. The elements in Zone B are offset by 90° between each

element (accomplished by combining alternating 0° and 90° paddle elements). All remaining details of the extrusion experiments are provided in the discussion section. Each experiment processed anywhere between 20-400 grams of material.

X-Ray Powder Diffraction (XRPD)

The diffractometer (PANanlytical X'pert, Philips) was equipped with a $CuK\alpha$ source (λ = 1.54056 Å) operating at a tube load of 45 kV and 40 mA. The divergence slit size was 1/4°, while the receiving slit and the detector slit, were 5.0 mm, and 0.1 mm respectively. A small amount of sample was loaded onto Si 510 zero-background sample holder and scanned between 3 and 40° (2θ) with a step size of 0.008 and a step time of 15.2 s/step in the continuous mode. Data was collected by a high-resolution sealed proportional detector. The Si (111) with a diffraction peak at 28.44° 2θ was used as a standard to calibrate the instrument.

Differential scanning calorimetry (DSC) and Thermogravimetric analysis (TGA)

DSC measurements were conducted in crimped Aluminum pans using a Q200 (TA Instruments, NewCastle, DE) unit under 50 mL/min N2 purge. 3 to 5 mg samples were tested each time. Standard DSC scan using a heating rate of 10 °C /min was used. Indium was used as the calibration standard.

For phase diagram measurements 5 to 10 mg of the appropriate blend samples were tested using a heating rate of 5 °C /min. The phase diagram measurements were made by in two stages: (a) combining AMG 517 and the cocrystal and (b) Combining sorbic acid and the cocrystal. This method was found to provide more unambiguous results than simply starting with AMG 517 and sorbic acid.

TGA measurements were conducted in Aluminum pans using a Q500 (TA Instruments, NewCastle, DE) unit under 50 mL/min N2 purge. A heating rate of 10 °C/min was used for all TGA runs.

Solid State Nuclear Magnetic Resonance (SSNMR)

All SSNMR measurements were conducted using a Bruker DSX spectrometer operating at a ^1H resonance frequency of 600 MHz. A Bruker 2.5 mm or 4-mm double resonance

magic angle spinning (MAS) probe head was used to record all NMR data. A sample spinning speed of 14 to 35 kHZ was used. The presence of a trifluoromethyl moiety in the AMG 517 structure, allows for the investigation of samples by ^{19}F SSNMR. As ^{19}F nucleus has high natural abundance and sensitivity, traditional single pulse NMR experiments can provide rapid quantitative information about the presence of different phases in the sample. ^{1}H 90° pulse length of 2.5 μs and a cross polarization contact time of 2 ms were employed. ^{1}H decoupling was achieved with a spinal 64 sequence using a pulse length of 5 μs. A recycle delay of 10 seconds was used. Teflon with chemical shift of -122 ppm was used as the chemical shift reference.

Particle Size Distribution by Dry Dispersion Laser Diffraction

Particle-size analysis was performed on a Sympatec Helos H1782 equipped with a Rodos/M dry disperser and Aspiros Micro Dosing System feeder. Disperser injector diameter was 4 mm and feeding rate was 30 mm/sec. Primary dispersing pressure of 1.0 bar and a R3 lens (0.9 to 175 μm) was used. The start/stop trigger threshold was set at a minimum optical concentration of <0.1%.

BET Surface Area

BET surface area measurement was performed on a Micromeritics Tristar II Surface Area and Porosity Analyzer 3020 using Krypton absorbate. Adsorption volumes were determined at multiple points from 5 to 25% p/p0 pressure range at 77.5 Kelvin.

Bulk and Tap Density

Tap density was determined using a Varian P/N 50-1200 tap density tester following USP method. API, sieved through #30 mesh and was dispensed into the 100mL graduated cylinder. The volume and weight were recorded for bulk density analysis. The cylinder was tapped and the tap density calculated.

Scanning Electron Microscopy

SEM images were acquired from an EVO® MA15 with LaB6 source Carl Zeiss Microscopy system. Sample was loaded on a carbon tape adhered to aluminum pin stub and sputter coated with gold and palladium.

Flow Function

The flow function was determined using the RTS-XS Ring Shear Cell with an XSMV4 cell. The drug substance was passed through a 30 mesh screen prior to testing to ensure that the material was delumped. Measurements were performed at various consolidation pressures (1, 2, 3, and 6 kPa), and flow functions were recorded.

HPLC

A reversed-phase HPLC gradient analysis was performed on AMG 517 freebase, SCC, and TSEC samples. The analysis was run on an Agilent HP1100 series HPLC system using a Phenomenex 150 x 4.6 mm, 3 micron Luna C18(2) HPLC column. The method was validated for SCC, and it is stability indicating and capable of separating most of major impurities. The method is capable of accurately quantifying AMG 517 in SCC and TSEC samples. To demonstrate the stability of the TSEC sample, it was stressed at 60°C closed condition and 40°C/75%RH open condition for 4 weeks and analyzed via HPLC to assay for chemical purity and XRD to assay for physical stability.

Results and Discussion

AMG 517 was developed as a potent and selective antagonist of VR1 indicated in the treatment of acute and chronic pain. The structure of AMG 517 is shown in Figure 2. Based on superior in-vivo performance following oral administration in male Sprague-Dawley rats, the sorbic acid cocrystal of AMG 517 was selected for development over AMG 517 freebase.[4] About 15 Kgs of the cocrystal was synthesized via solution crystallization (SCC) to support development. The XRPD and DSC data of SCC are shown in Figure 3. The XRPD data of the sample is in good agreement with the powder pattern calculated from the single crystal structure. The singe crystal structure of the material has been solved and the details are reported in Reference 4. The first endotherm

with an onset temperature of 204 .8 °C in the DSC thermogram represents the melting of the cocrystal while the second endotherm with the onset of 223.3 °C represents the melting of the residual free acid. The data show that the cocrystal is an anhydrous crystalline solid.

I. Cocrystal synthesis using ball milling

Prior to extrusion experiments, ball milling was conducted on a 500 mg scale to determine if mechanical action could lead to cocrystal formation. Ball milling was conducted at 30 Hz, the highest available frequency in the model used. Samples removed from the ball mill at different times were analyzed by ^{19}F SSNMR. By the 5-minute milling time point conversion >80% was seen. After ball milling for 30 minutes, complete conversion to cocrystal was observed. Based on the data obtained from ball milling it is clear that AMG 517-sorbic acid cocrystal can be easily generated by mechanical action and as such it was decided use AMG 517-sorbic acid cocrystal system as an example case to illustrate the scalability of cocrystal production using TSE. Since an abundance of high quality SCC was also available, it would be possible to make head to head comparison of TSEC with SCC material in order to gauge the effectiveness of TSE as an alternative to solution based processes.

II. Optimization of experimental parameters for TSE

Screw design, temperature, feed rate and the RPM of the screws are the primary experimental parameters that can affect cocrystal conversion in the extruder. In previous studies with other cocrystal systems, the effect of screw design on cocrystal conversion was examined by using several designs intended to provide varying degree of mixing and conveying.[22] From these studies, it was determined that for mechanochemical applications a screw configuration that provides for intense mixing where new surfaces are continuously generated was crucial to achieve high conversions. Based on these prior observations, the screw design that provides for high mixing was used for all experiments in this study.

The most important factor that can influence cocrystal formation is the temperature in the extruder barrel. The effect of temperature on cocrystal conversion was studied by

varying the temperature in the barrel between 10 and 135 °C. For these experiments, the feed rate was kept at 5% and the screw RPM was maintained at 25. ^{19}F SSNMR analysis of samples from each of these runs is shown in Figure 4. The preblend sample prior to extrusion, containing stoichiometric equivalents of the two staring materials, did not show any conversion to the cocrystal. This shows that the mechanical action provided by TSE is critical for cocrystal formation. The data also shows that even at the lowest temperature of 10 °C, a high conversion to the cocrystal is achieved. However, complete conversion to the cocrystal was only achieved at 115 °C, indicating that increasing temperature only improves the kinetics of the process. All temperatures used in this study up to 115 °C are less than the individual melting points of AMG 517 (226.9 °C) and sorbic acid (133.5 °C). As the cocrystal formation occurs for all temperatures used it indicates that mechanism of cocrystal formation may not be mediated by a liquid phase formation due to the eutectic temperature. Based on previously published studies, it was found that cocrystal conversion may or may not be mediated by eutectic formation.[22] For example, eutectic formation was clearly shown to mediate cocrystal formation for the Nicotinamide-Cinnamic acid system. However, mechanism based on eutectic formation was found to be unlikely for Caffeine-oxalic system. While it seems unlikely that eutectic formation leads to cocrystal production in the case of AMG 517-sorbic acid system, it was decided to investigate this further by developing a complete phase diagram for the system.

A phase diagram for the AMG 517-sorbic acid system is shown in Figure 5. The phase diagram is typical of what is expected of a binary system with compound formation. The solid lines represented fits to the Schroeder-Van Laar equation which relates the temperature at which crystallization occurs (T) to the mole fraction of the solute (χ):

$$T = \left(\frac{1}{T_m^*} - \frac{R \ln \chi}{\Delta H_{fus}} \right)$$

Where T_m^* and ΔH_{fus} are the melting and the heat of fusion of the pure component and R is the universal gas constant. The equation fits for the cocrystal-freebase part of the phase diagram well while the fit is not good for sorbic acid-cocrystal part of the phase diagram. This indicates that ideal behavior assumed by the Schroeder-Van Laar equation is not applicable for the sorbic acid-cocrystal system.

Two eutectic points are evident from the data: (a) $T_{eu1} \sim 404$ °K (131 °C) between sorbic acid and AMG 517-sorbic acid cocrystal and (b) $T_{eu2} \sim 467$ °K (194 °C) between AMG 517-sorbic acid cocrystal and AMG 517. Both these eutectic points are higher than most of the temperatures used in the extrusion study. Thus formation of the cocrystal in the extruder is not mediated by eutectic formation. This still leaves the question of the mechanism responsible for cocrystal formation open. To explain the mechanism of mechano-chemical reactions, usually an intermediate phase is invoked which can be (a) liquid state, (b) vapor state or (c) amorphous state. The existence of an intermediate liquid state in the formation of AMG 517-sorbic acid cocrystal has been ruled out through phase diagram measurements. The vapor pressure of these compounds does not lend themselves to sublimation and therefore the presence of an intermediate vapor phase in mediating cocrystal formation is also unlikely. Nair et. al.[26] and Friscic et. al.[27] have proposed that an amorphous intermediate state could mediate cocrystal formation. Surface amorphization of materials through high shear provided in the mixing zones of the extruder is possible. This amorphous phase, owing to enhanced mobility, could then mediate cocrystal formation. Additionally, new surfaces are continuously being generated in the TSE process which could facilitate propagation of cocrystal formation through an amorphous intermediate state. While there is no direct evidence of surface amorphous formation, this seems to be the most likely mechanism driving cocrystal formation in the case of AMG 517-sorbic acid system.

The effect of feed rate and RPM on cocrystal conversion was investigated at 100 °C. The feed rate was varied from 5 to 15% while keeping the RPM constant at 100. Based on XRPD data it was clear that there is residual starting material in all cases with the lowest amount of starting material seen for the 5% feed rate. These results show that a high RPM of 100, even the lowest feed rate would not provide complete conversion to the cocrystal. Similarly screw speeds of 25, 50 and 100 RPM were investigated at a feed rate of 5% to understand the effect of residence time on conversion. It is assumed that at the lower the RPM there is a longer residence time in the extruder. In line with the previous observations, the lower RPM's of 25 and 50 provided near complete conversion while the 100 RPM shows the presence of unreacted starting material. The XRPD data for screw speed and RPM variation is shown in Figure 6. These data indicate that the extent of

conversion to the cocrystal shows a strong dependence on temperature while showing moderate dependence on feed rate and screw speed.   For the final scale up, the following conditions were chosen: 115 °C, 5% feed rate, and 50 RPM. The 115 °C temperature and a feed rate of 5% were chosen to provide complete conversion to cocrystal. The screw speed was set in the middle of the range to 50 RPM to ensure adequate residence time for full conversion while at the same time providing for reasonable process duration.

III. Production of AMG 517-sorbic acid cocrystal by TSE

Stoichiometric quantities of AMG 517 and sorbic acid were mixed together in a bottle and blended by hand.   The pre-blended material was fed through a hopper into the extruder at a feed rate of 5% while the barrel was maintained at 115 °C. The extruder was run for a total time of 4 hours and 16 minutes. Samples were periodically collected from extruder as time point composites.   Frequent sampling in 5 minute intervals was done for the first 15 minutes and sampling frequency was reduced to an hourly basis from one through four hours.   These samples were analyzed by XRPD and ^{19}F SSNMR to check for extent of conversion to the cocrystal. At all time points complete conversion to the cocrystal was observed (data not shown) indicating the scale up process performs uniformly over time. Total converted cocrystal collected was approximately 140 grams. As this is a continuous process, the extrusion process can simply be run for a longer duration to generate more material. Furthermore, a higher throughput can be achieved by moving to a larger diameter twin screw extruder (e.g. move from a 16 mm extruder 27 mm extruder). The essential TSE parameters for the run are summarized in Table 1. The RPM, temperature, and feed rate are tightly controlled during the extrusion process. The only observation during the scale up run was the output rate decreased from about 0.63 g/min to 0.49 g/min. This decrease in output over time is due to the feeder getting caked with pre-blend which in turn decreases the conveying efficiency. The feeder deficiency can be easily mitigated by moving from a volumetric based feeder to a gravimetric based feeder.   Nevertheless, the experiment demonstrated that cocrystal production can be successfully scaled using TSE.

IV. Comparison of TSEC and SCC

<u>Solid state properties</u>: Figure 7a shows XRPD patterns of TSEC and SCC in comparison with the powder pattern calculated from the single crystal structure. The experimental XRPD patterns of the TSEC and SCC materials are in good agreement with the calculated powder pattern indicating that the cocrystal is formed in both processes. Using the quantitative HPLC analysis the conversion of AMG 517 freebase to the AMG 517-sorbic acid cocrystal in the TSEC was calculated to be higher than 99%. The percent conversion of the freebase to the cocrystal was found to comparable between the TSEC and the SCC samples. DSC thermograms of the TSEC in comparison with the freebase and sorbic acid are shown in Figure 7b. The peak melting temperature of the cocrystal was found to be in-between that of the starting components. Thus, thermal data provide further confirmation of the cocrystal formation by the TSE process. Based on these data, twin screw extrusion was found to be a viable option for producing AMG 517-sorbic acid cocrystals.

<u>Chemical stability of TSEC and SCC:</u> As the TSE process involves the use of high temperature to force complete conversion to the cocrystal, the question regarding the chemical stability of the final material has to be addressed. The melting point of the cocrystal was found to be 207 °C and therefore the thermal excursion of the material to 115 °C for a short period (< 6 minutes) in the extruder is unlikely to cause any thermal degradation. Nevertheless, a comprehensive head to head stability analysis of the TSEC and SCC was initiated at accelerated storage conditions to assess chemical liability of the materials. The stability data are summarized in Table 2. The data shown in Table 2 are in % relative area basis. The TSEC sample is of comparable purity to the SCC sample. However, the SCC sample shows a lesser percentage of total impurities than the TSEC sample. This is due to the fact that crystallization in solution is able to reject impurities while TSE based crystallization is unable to do so. This is one of the drawbacks of solid state method of producing cocrystals in that chemical purification is not possible. Additionally the TSEC sample stressed under accelerated conditions show excellent stability.   The data presented show that TSE can be used to produce high quality

cocrystals provided that starting AMG 517 freebase is clean. The high temperature used in the TSE process does not produce any additional impurities in the sample.

Mechanical properties: A comparison of the mechanical properties of TSEC and SCC are provided in Table 3. The SEM micrographs of particles are shown in Figure 8 and the particle size distribution as measured by dry dispersion laser diffraction is shown in Figure 9. SCC particles have a rod shape morphology with significant particle aggregation while the TSEC particles have irregular morphology with significant particle aggregation. SEM data also show that while SCC crystals have smooth surfaces, TSEC crystals have corrugated surfaces. The morphological and textural differences between the samples are in line with the expectation based on the different processes that were used to generate these crystals. In order to break the aggregation, 1 bar dispersing pressure was used in the PSD measurements. The PSD measurements show that TSEC have a broader distribution than SCC. The PSD metrics for the two samples are shown in Table 3. The D90 for the TSEC sample is nearly 1.8X that of the SCC sample, indicating presence of bigger particles for TSEC sample. The measured surface area of the samples is contrary to the expectation based on PSD measurement. It would be expected that the SCC sample would have the higher surface area as it has the lower particle size. However, the data shows that the TSEC sample has 3X the surface area of the SCC sample. This result can be rationalized through the surface difference between the two samples as seen in the SEM images. The TSEC sample that presents a highly corrugated surface and hence a larger surface area than the SCC samples which have smooth surfaces. This is one of the advantages of the TSE process, in that it can readily produce material with higher surface area due to the mechanical action. The use of TSE process may eliminate the need for secondary processing such as milling to improve the surface area.

In addition to the surface area improvement, TSEC material also shows improved bulk density and flow function coefficient. The flow function data for SCC and TSEC are shown in Figure 10. The flow of the TSEC sample is classified as *easy flowing* when compared SCC material that is classified as *very cohesive*. The improvements achieved for the TSEC can again be rationalized through the densification that can be achieved

when using the TSE process. The improvements in bulk density and flow characteristics of the active can lead to improved performance in the drug product. For example, the improvements achieved by using the TSE process can be advantageous when making high strength tablets with increased drug loads using dry granulation. There a few reports in literature of cocrystallization improving the mechanical performance of the pharmaceutically active ingredient. In this report it is demonstrated that not only cocrystallization but also the method of cocrystallization is important when considering improvements in mechanical properties.

Finally, the use of solvents in making the cocrystal has been completely eliminated by the use of TSE process. For example, the current process of making the SCC uses nearly a liter of solvent to make 100 grams of material. The entire need for the solvent has been obviated by moving to a continuous mechano-chemically scalable process. Therefore in addition to the aforementioned advantages, TSE is a green chemistry process.

Conclusions

The scale up of AMG 517-sorbic acid cocrystal was demonstrated using TSE. A high mixing screw design was used to produce the cocrystals, as mixing in the extruder was demonstrated to be critical for cocrystal formation. The mechanism of cocrystal formation in the extruder was found not to be mediated by eutectic formation. However, temperatures greater than 100 °C were required to ensure complete conversion to the cocrystal. Feed rate and screw speed were found to have only a moderate influence on cocrystal conversion. TSEC were found to have improved surface area, bulk density, and flow properties when compared to SCC. In addition, the entire need for the solvent has been obviated by moving to TSE as a production method. TSE can be considered to be a continuous, efficient, scalable, and an environmentally friendly process for the production of cocrystals.

References

1. A. D. Bond, *Cryst. Eng. Comm* 2007, **9**, 833-834.
2. G. R. Desiraju, *Cryst. Eng. Comm* 2003, **5**, 466-467.
3. J. D. Dunitz, *Cryst. Eng. Comm* 2003, **5**, 506.
4. A. Bak, A. Gore, E. Yanez, M. Stanton, S. Tufekcic, R. Syed, A. Akrami, M. Rose, S. Surapaneni, T. Bostick, A. King, S. Neervannan, D. Ostovic and A. Koparkar, *J. Pharm. Sci.* , 2008, **97**, 3942-3956.
5. R. Banerjee, P. M. Bhatt, N. V. Ravindra and G. R. Desiraju, *Crystal Growth & Design*, 2005, **5**, 2299-2309.
6. A. M. Chen, M. E. Ellison, A. Peresypkin, R. M. Wenslow, N. Variankaval, C. G. Savarin, T. K. Natishan, D. J. Mathre, P. G. Dormer, D. H. Euler, R. G. Ball, Z. Ye, Y. Wang and I. Santos, *Chem. Commun. (Cambridge, U. K.)* 2007, 419-421.
7. S. L. Childs, L. J. Chyall, J. T. Dunlap, V. N. Smolenskaya, B. C. Stahly and G. P. Stahly, *J. Am. Chem. Soc.* , 2004, **126**, 13335-13342.
8. D. J. Good and N. Rodriguez-Hornedo, *Crystal Growth & Design*, 2009, **9**, 2252-2264.
9. D. P. McNamara, S. L. Childs, J. Giordano, A. Iarriccio, J. Cassidy, M. S. Shet, R. Mannion, E. O'Donnell and A. Park, *Pharmaceutical Research*, 2006, **23**, 1888-1897.
10. J. F. Remenar, S. L. Morissette, M. L. Peterson, B. Moulton, J. M. MacPhee, H. R. Guzman and O. Almarsson, *J. Am. Chem. Soc.* , 2003, **125**, 8456-8457.
11. N. Variankaval, R. Wenslow, J. Murry, R. Hartman, R. Helmy, E. Kwong, S.-D. Clas, C. Dalton and I. Santos, *Crystal Growth & Design*, 2006, **6**, 690-700.
12. S. Karki, T. Friscic, L. Fabian, P. R. Laity, G. M. Day and W. Jones, *Advanced Materials (Weinheim, Germany)*, 2009, **21**, 3905-3909.
13. C. C. Sun and H. Hou, *Crystal Growth & Design*, 2008, **8**, 1575-1579.
14. A. V. Trask, W. D. S. Motherwell and W. Jones, *Chem. Commun. (Cambridge, U. K.)* 2004, 890-891.
15. A. V. Trask, W. D. S. Motherwell and W. Jones, *Crystal Growth & Design*, 2005, **5**, 1013-1021.
16. R. A. Chiarella, R. J. Davey and M. L. Peterson, *Crystal Growth & Design*, 2007, **7**, 1223-1226.
17. S. J. Nehm, B. Rodriguez-Spong and N. Rodriguez-Hornedo, *Crystal Growth & Design*, 2006, **6**, 592-600.
18. N. Rodriguez-Hornedo, S. J. Nehm, K. F. Seefeldt, Y. Pagan-Torres and C. J. Falkiewicz, *Mol. Pharm.* , 2006, **3**, 362-367.
19. A. Ainouz, J.-R. Authelin, P. Billot and H. Lieberman, *Int J Pharm FIELD Full Journal Title:International journal of pharmaceutics*, 2009, **374**, 82-89.
20. A. Y. Sheikh, S. Abd. Rahim, R. B. Hammond and K. J. Roberts, *CrystEngComm* 2009, **11**, 501-509.

21. T. Friscic, A. V. Trask, W. Jones and W. D. S. Motherwell, *Angew. Chem., Int. Ed.* , 2006, **45**, 7546-7550.
22. D. Daurio, C. Medina, R. Saw, K. Nagapudi and F. Alvarez-Nunez, *Pharmaceutics*, 2011, **3**, 582-600.
23. C. Medina, D. Daurio, K. Nagapudi and F. Alvarez-Nunez, *J. Pharm. Sci.*, 2010, **99**, 1693-1696.
24. R. S. Dhumal, A. L. Kelly and A. R. Paradkar, *Journal of Pharmacy and Pharmacology*, 2010, **62**, 1418-1419.
25. R. S. Dhumal, A. L. Kelly, P. York, P. D. Coates and A. Paradkar, *Pharmaceutical Research*, 2010, **27**, 2725-2733.
26. A. Jayasankar, A. Somwangthanaroj, Z. J. Shao and N. Rodriguez-Hornedo, *Pharmaceutical Research*, 2006, **23**, 2381-2392.
27. I. Halasz, A. Puškarić, A. J. S. Kimber, P. J. Beldon, A. M. Belenguer, F. Adams, V. Honkimäki, R. E. Dinnebier, P. Bhavanita, W. Jones, V. Štrukil and T. Friscic, *Angew. Chem., Int. Ed.* , 2013, **125**, 11752–11755.

List of Figures

List of Tables

Table 1: Experimental TSE parameter variation during scale up.

TSE Parameter	Mean (RSD)	Min-Max
Torque, N-m	6.9 (2.3)	3-19
Temperature, C	115 (0)	-
RPM	49.5 (2.1)	43-57
Feed rate, %	4.96 (0.27)	2-6

Table 2. Chemical stability of TSEC under accelerated storage conditions

	Freebase (T=0)	TSEC (T=0)	TSEC 40C/75%RH	TSEC 60C/2weeks	SCC (T=0)
AMG 517	98.90	98.92	98.8	98.86	99.50
% Total Impurities	0.90	0.90	0.94	0.93	0.34

Table 3: Comparison of the mechanical properties of TSEC and SCC

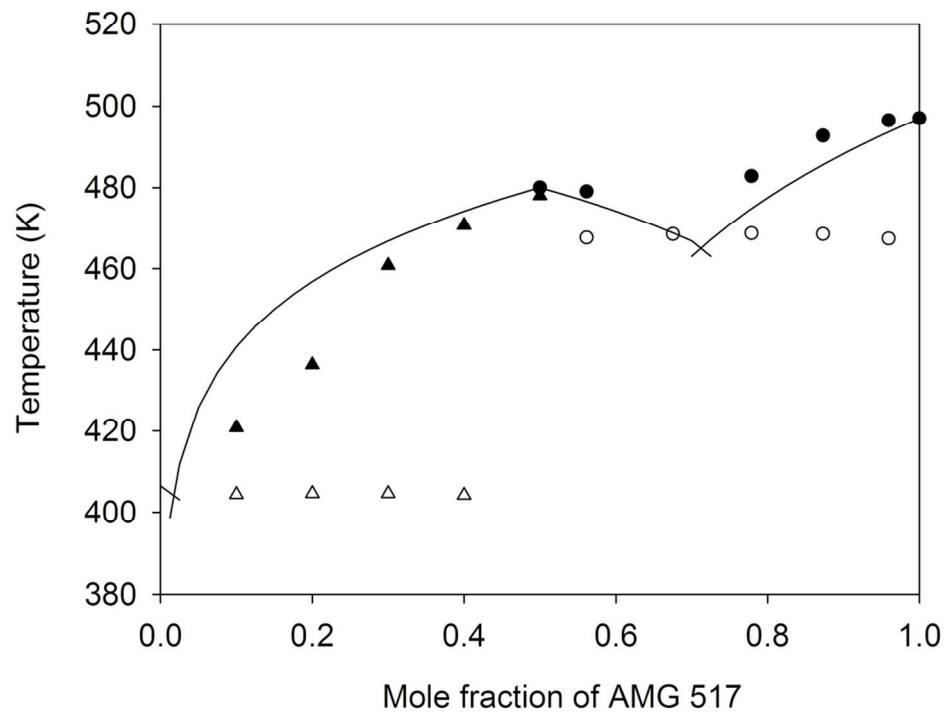| Property	Solution Co-crystal	TSE Co-crystal
PSD	D_{10} = 1.7 µm D_{50} = 6.9 µm D_{90} = 30.5 µm M_v = 12.4 µm	D_{10} = 1.4 µm D_{50} = 9.8 µm D_{90} = 53.4 µm M_v = 19.5 µm
Surface area	0.9 m^2/g	2.9 m^2/g
FFC @ 2 kPa	1.5	4.4
Bulk density	0.21 g/cc	0.49 g/cc
Tap density	0.38 g/cc	0.85 g/cc
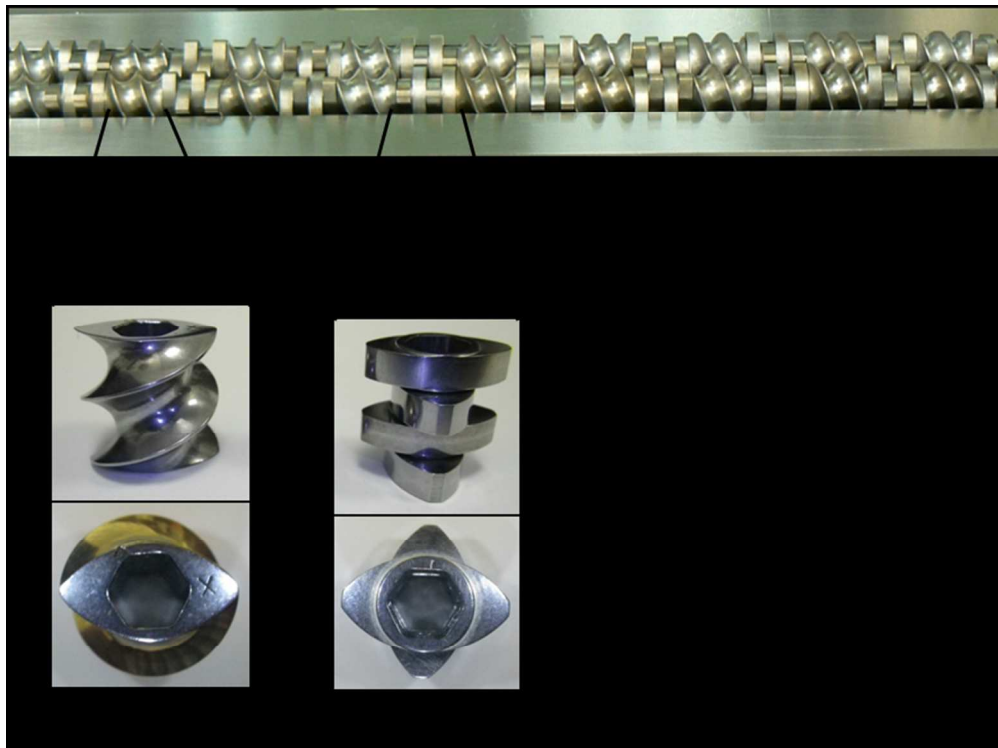
150x112mm (150 x 150 DPI)
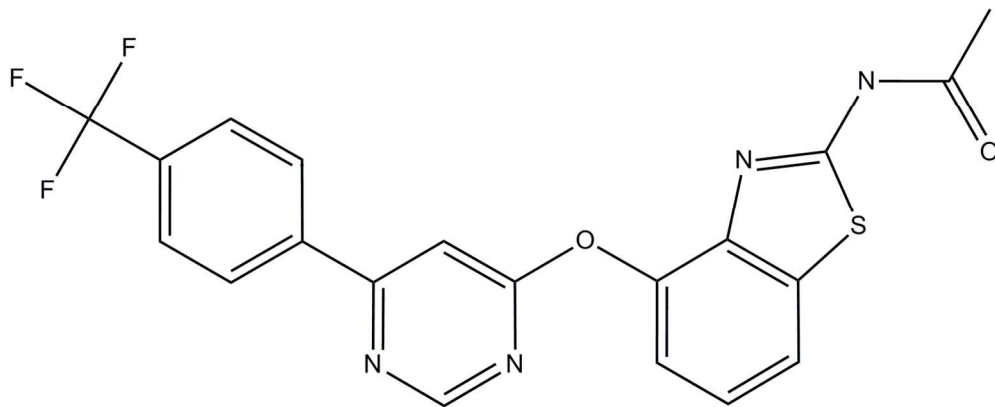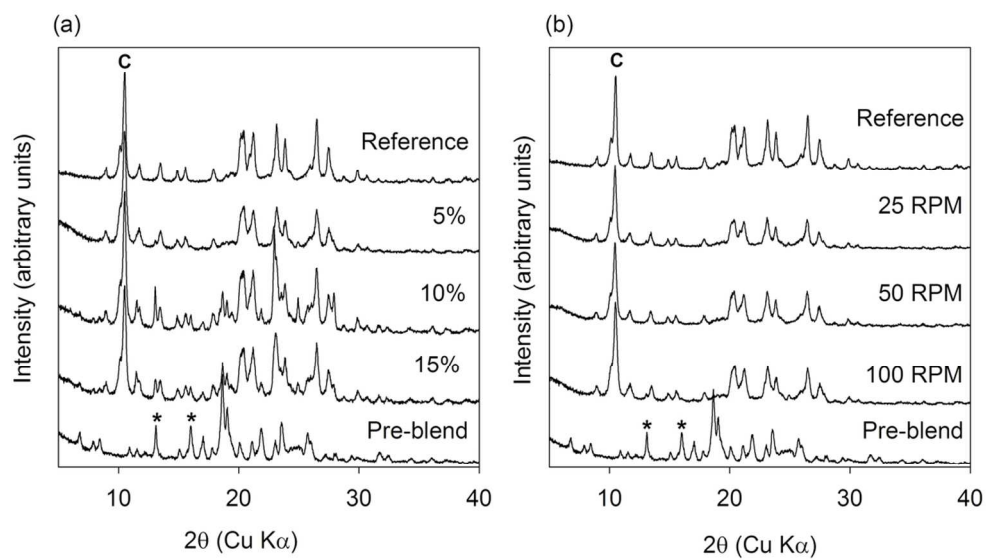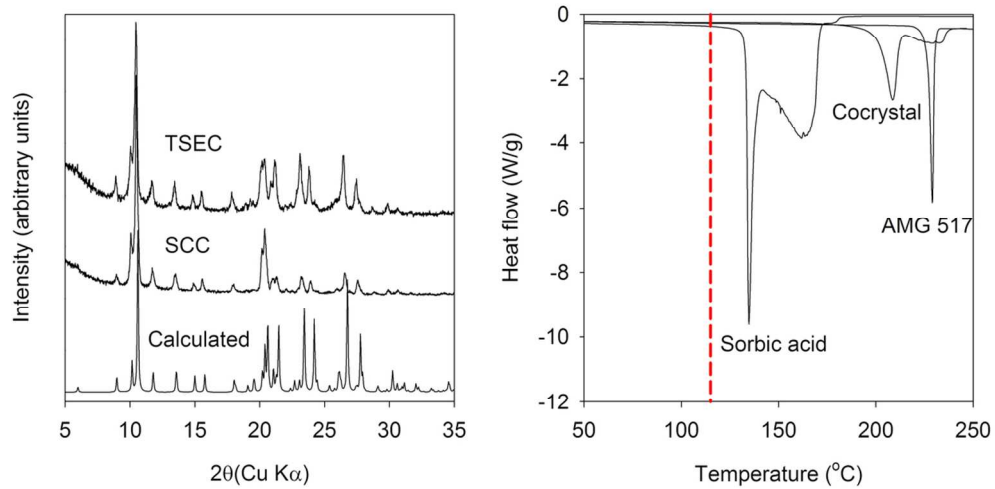
137x56mm (300 x 300 DPI)
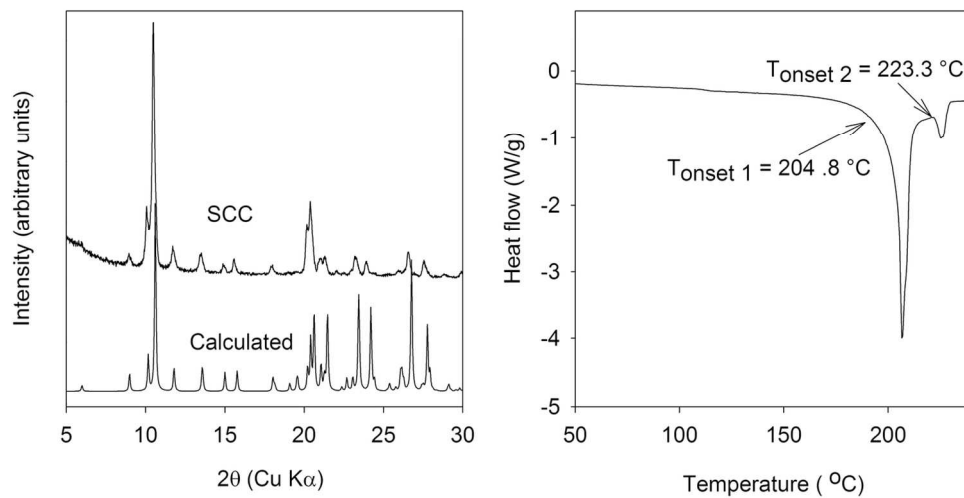
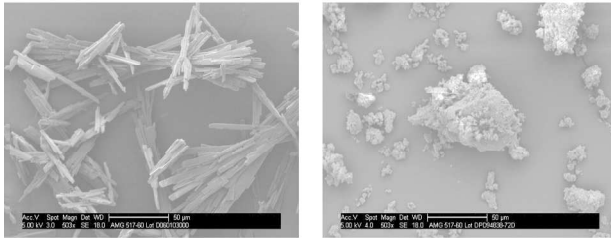129x87mm (300 x 300 DPI)
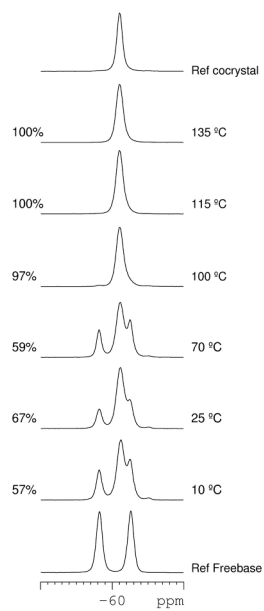
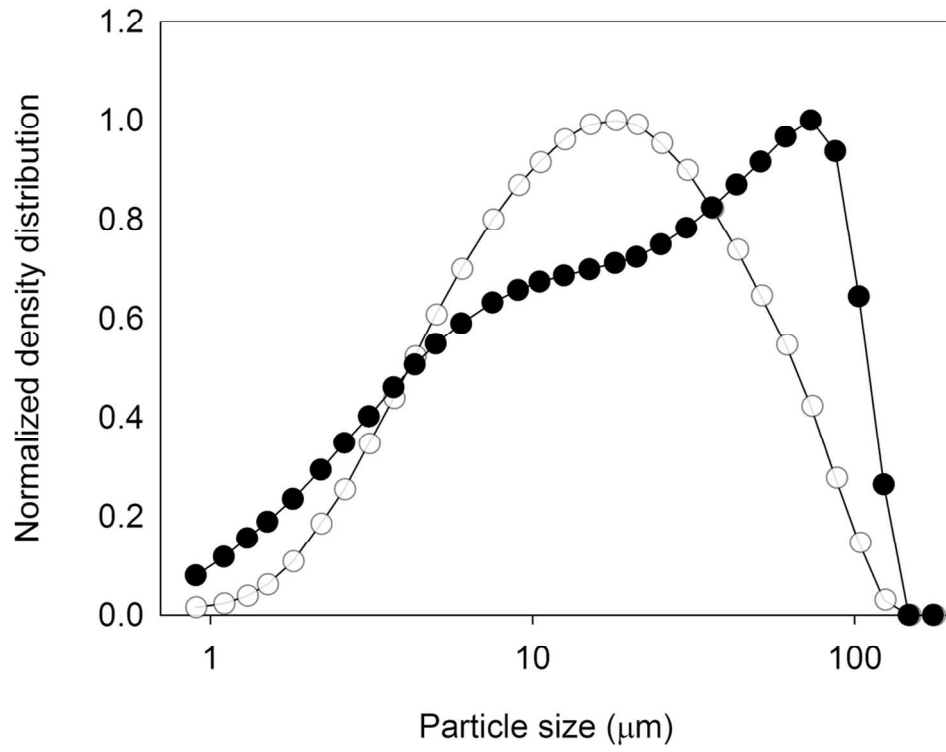215x166mm (300 x 300 DPI)

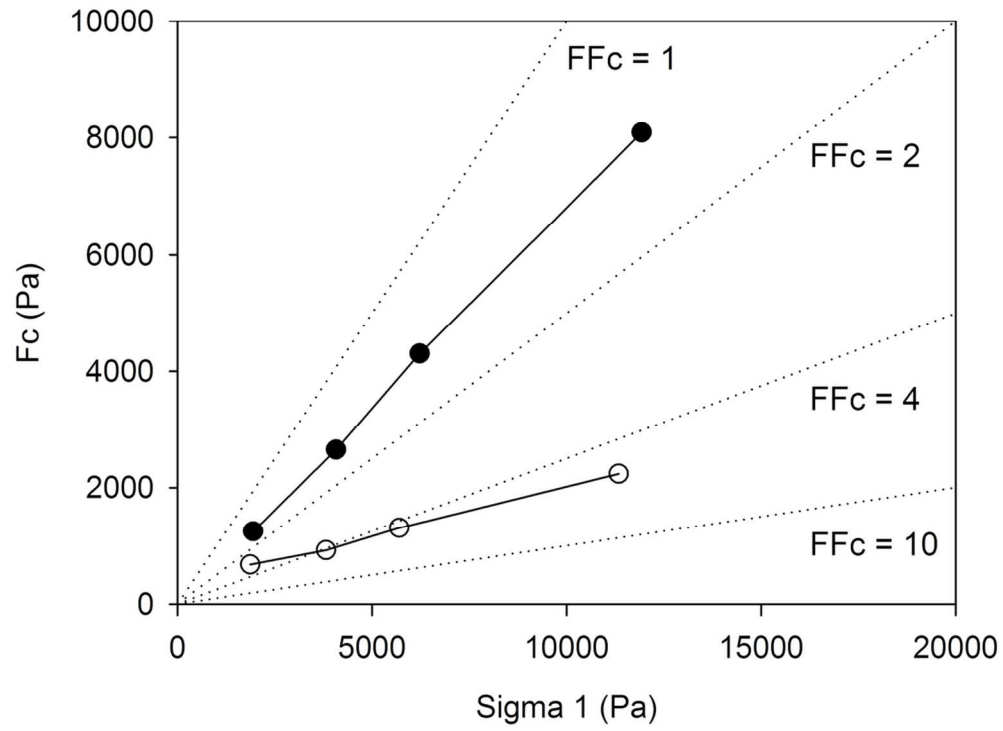105x83mm (300 x 300 DPI)

106x62mm (300 x 300 DPI)

106x57mm (300 x 300 DPI)

215x93mm (300 x 300 DPI)

106x88mm (300 x 300 DPI)

105x85mm (300 x 300 DPI)